RSC Advances

PAPER

View Article Online
View Journal | View Issue

Cite this: *RSC Adv.*, 2022, **12**, 5255

Double noncovalent network chitosan/hyperbranched polyethylenimine/Fe^{3+} films with high toughness and good antibacterial activity†

Kaijie Xu, Qingyin Dai, Kaiqiang Dong, Ningsi Wei and Zhiyong Qin*

Received 5th November 2021
Accepted 20th January 2022

DOI: 10.1039/d1ra08121g

rsc.li/rsc-advances

The application of pure chitosan films is significantly limited due to their poor mechanical properties. In this study, a novel type of chitosan/hyperbranched polyethylenimine (CHP) and chitosan/hyperbranched polyethylenimine/Fe^{3+} (CHPF) films with high toughness and good antibacterial activity were prepared through a noncovalent crosslinking method. From the tensile test results, the strain and toughness of the CHP film increased by 798.1% and 292.3%, respectively, compared with pure chitosan film, after the addition of 20% hyperbranched polyethylenimine (HPEI). The addition of trace metal iron ions (3 mg) forms a metal coordination bond with the amine group on HPEI, as well as the hydroxyl group and amine group on chitosan, and develops a double noncovalent bond network structure with hydrogen bonding, which further enhances the mechanical tensile strength of the chitosan-based film, with an increase of 48.4%. Interestingly, HPEI and Fe^{3+} can be used as switches to increase and decrease the fluorescence property of chitosan, respectively. Furthermore, the CHP and CHPF films showed good antibacterial activity against *S. aureus* and *E. coli*.

1 Introduction

In the past decades, researchers have had a great interest in biomass-based multifunctional materials, such as cellulose, rosin, lignin, plant oils and polysaccharides, because of their abundance and sustainability, which can solve the problems caused by the dependence on fossil resources.[1–3] Chitosan is a linear amino polysaccharide.[4] Chitosan-based films with excellent biocompatibility, biodegradability, sustainability, and good complexing ability have been widely used in tissue engineering, wastewater decontamination, food packaging and other fields.[5–7]

However, chitosan-based films exhibit disadvantages of poor mechanical properties and inferior water vapor barrier properties, which limit their application in the biomedical field and food packaging, among others.[7] Due to rigid molecular interaction and the strong hydrogen bond between chitosan matrix molecules, chitosan films exhibit poor toughness. Therefore, considerable efforts have been made to improve the toughness of chitosan films, such as adding flexible polymers for physical blending,[8,9] adding inorganic nanoparticles,[10–16] chemical crosslinking,[8,17–21] and chemical modification.[22–25] For example, the addition of polyvinyl alcohol[9,17,26] and poly-(lactic acid)[16,27,28] can enhance the strain and toughness of chitosan-based films by forming hydrogen bonds between flexible polymers and chitosan molecules. Hyperbranched polyethylenimine (HPEI) is a water-soluble flexible polymer composed of a large number of amino and imino groups.[3,29] Thus, it is an ideal component to improve the toughness of chitosan-based films and maintain their flexibility. Li *et al.* attempted to combine HPEI with soy protein isolate (SPI) molecules using hydrogen bonds, and the tensile strength of the SPI/HPEI film increased from 2.79 MPa to 8.29 MPa.[29]

Although the toughness of the chitosan films is improved by blending with flexible polymers, the mechanical strength will decrease accordingly, and a strategy is needed to achieve a balance between toughness and strength. Compared with single-network materials, double-network[30–33] materials exhibit better mechanical properties. When the first-network is a hydrogen bond network, the second-network is usually a chemical crosslink network, metal coordination network, or another noncovalent network. Yu *et al.* prepared a chitosan derivative/PVA blend film cross-linked with glutaraldehyde; the cross-linked film still exhibits better mechanical properties and antibacterial activities.[8] Moreover, cross-linked hydrogels have been formed *via* the reaction between catechol-modified polyethylene glycol polymers and Fe^{3+}, and the resulting hydrogels are shown to have high elastic moduli and good self-healing properties.[34] Different types of noncovalent bonds (hydrogen bonds, π–π stacking, host–guest interaction, ionic interaction, and metal coordination) can also be used in combination to construct different multi-physical networks. Zhang *et al.* fabricated a fully physical double-network hydrogel by the

School of Resources, Environment and Materials, Guangxi University, Nanning, 530004, China. E-mail: qinzhiyong@gxu.edu.cn

† Electronic supplementary information (ESI) available. See DOI: 10.1039/d1ra08121g

synergistic effect of multiple hydrogen and ionic bonds.[35] The synergistic effect of double-networks can enhance the toughness of the material at the expense of a small part of the mechanical strength, while also endowing the material with other functions.

In this study, double noncovalent network chitosan-based films were prepared. The addition of HPEI led to the first noncovalent network (hydrogen bond) being formed between chitosan molecules and HPEI, and the second noncovalent network (metal coordination) can be further developed by introducing Fe^{3+}. The synergistic effect of hydrogen bonds and metal coordination bonds can allow chitosan-based films to maintain their tensile strength and endow good strain resistance and toughness, which provide a solution to the problem of the high strength but poor toughness of pure chitosan film. Interestingly, the addition of HPEI and Fe^{3+} can synergistically tune the mechanical properties of chitosan-based films, while HPEI and Fe^{3+} can be used as switches to increase and decrease the fluorescence property of chitosan, respectively. Furthermore, CHP and CHPF films showed good antibacterial activity against *S. aureus* and *E. coli*.

2 Materials and methods

2.1 Materials

Chitosan (viscosity 100–200 mpa s) with a degree of deacetylation ≥95% was purchased from Macklin Biochemical Reagent Co., Ltd (Shanghai, China). Iron(III) nitrate nonahydrate ($Fe(NO_3)_3 \geq 98.5\%$) was purchased from Macklin Biochemical Reagent Co., Ltd (Shanghai, China). Hyperbranched polyethylenimine (HPEI, 97%) was obtained from Sigma Aldrich Reagent Co., Ltd (Shanghai, China). *Staphylococcus aureus* ATCC 25923 and *Escherichia coli* ATCC 25922 were purchased from Huankai Microbial Technology Co., Ltd (Guangdong, China). The studied bacteria were grown in MHB at 37 °C for 24 h to 10^7 CFU mL^{-1} at the mid-log phase before the tests.

2.2 Preparation of the CS, CHP and CHPF films

1 g chitosan powder was dissolved in a 1% acetic acid solution and magnetically stirred for 12 h to make a uniform solution (100 mL). Different contents of HPEI (0 g, 0.05 g, 0.10 g, 0.15 g, 0.20 g) were then dissolved in 5 mL deionized water and added to the chitosan solution, and the samples were correspondingly named CS, CHP-1, CHP-2, CHP-3, and CHP-4. Then, the samples were magnetically stirred in a water bath at 60 °C for 6 h and stirred at room temperature for 6 h to form a homogeneous mixed solution. After that, the solutions were transferred to Petri dishes ($\Phi = 12$ cm) and dried in a constant temperature and humidity box at 45 °C and 50% RH.

The preparation of CHPF films was similar to the previously mentioned CHP film preparation process. After adding HPEI to form a uniform solution, the prepared Fe^{3+} solution (5 mg mL^{-1}) was added to the CHP-4 solution. The samples with different Fe^{3+} content (0.5 mg, 1 mg, 2 mg, 3 mg, 6 mg) were named CHPF-1, CHPF-2, CHPF-3, CHPF-4, and CHPF-5, respectively. Then, the matrix was heated and magnetically stirred in a water bath at 60 °C for 1 h and magnetically stirred at room temperature for 12 h. Finally, they were transferred to Petri dishes ($\Phi = 12$ cm) and placed in a constant temperature and humidity box at 45 °C and 50% RH until the films were dried. Scheme 1 shows the specific chitosan-based film preparation processes. The detailed composition of the chitosan-based composite films is exhibited in Table S1.†

2.3 Characterization

The Fourier-transform infrared spectroscopy (FT-IR) analysis of the chitosan-based films was obtained using a spectrometer (Nicolet 7600 Nico-let Instrument Corporation, Madison, WI, USA) with an average of 32 scans recorded from 400 to 4000 cm^{-1} wavenumbers at a resolution of 4 cm^{-1}. X-ray photoelectron spectroscopy (XPS) was examined using an electron spectrometer (Thermo Fisher Scientific K-Alpha, USA) equipped with 100 W monochromatic A1 Kα irradiation. The test tube voltage and test energy were 15 kV and 1486.6 eV,

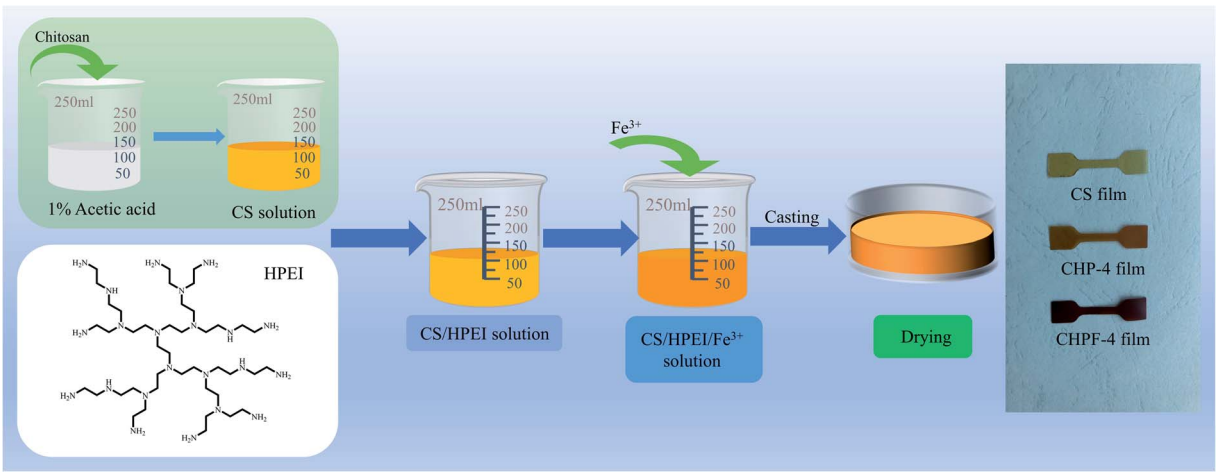

Scheme 1 Schematic representation of the development of the CS film, CHP films and CHPF films.

respectively. The thermal stability characteristics of the chitosan-based films were investigated using thermogravimetric analysis (TGA, Q50, TA Instruments, MA, USA). The fracture surface morphologies were evaluated using a Zeiss Sigma 300 scanning electron microscope (SEM) (ZEISS, Germany) and the surfaces were coated with a layer of gold before testing. Tensile testing was carried out on a ZHIQU 990 testing instrument (ZHIQU, China) with a crosshead speed of 2 mm min^{-1} at room temperature and a gage length of 18 mm. The samples were cut into a dumbbell shape through a cutter. Fluorescence measurements were recorded on a HORIBA FluoroMax-4 spectrofluorometer (HORIBA France). The UV-vis absorbance was recorded on a Macy UV-1800PC (Macy, China).

2.4 Antibacterial assay on the chitosan-based films

Single colony *S. aureus* and *E. coli* were resuscitated on LB medium, and the obtained bacteria were diluted to 10^7 CFU mL^{-1} with 0.3 mL phosphate buffered saline (PBS) (pH 6.8). 100 μL diluted bacterial solution was spread evenly on the surface of the culture medium with a spreading stick. Next, an Oxford cup was placed vertically on a flat plate and 200 μL chitosan-based solution was injected into the Oxford cup with a pipette gun. After 12 h incubation at 37 °C, the zone of inhibition was measured in millimeters with the help of a Vernier caliper.

3 Results and discussion

3.1 FT-IR analysis

The FT-IR spectra of pure chitosan film and the chitosan-based films are shown in Fig. 1. The peak located at 3190 cm^{-1} was assigned to the O–H and N–H stretching vibrations of chitosan.[36] The peak around 2858 cm^{-1} was attributed to the C–H stretching vibrations of alkane groups.[37] The peak at 1642 cm^{-1} corresponded to the C=O stretching of the acetyl group (amide-I) of chitosan and the band at 1538 cm^{-1} was attributed to the –NH bending and stretching (amide-II).[38] The peak at 1402 cm^{-1} was assigned to the scissoring vibrations of NH_2 groups and the absorption peak observed at around 1026 cm^{-1} corresponds to the saccharide structure of chitosan.[37,39] The spectra of the CHP films exhibited higher intensity at the peaks of 3190 cm^{-1}, 1538 cm^{-1}, and 1402 cm^{-1}. This was attributed to the introduction of a large number of NH_2 and NH groups after the addition of HPEI. It can be seen from Fig. 1(b) that after the addition of iron ions, the intensity of the spectra of the CHPF films at the peaks of 3190 cm^{-1}, 1538 cm^{-1}, and 1402 cm^{-1} was weakened, which was due to the formation of metal coordination bonds inside. Fig. S1† shows the FT-IR spectra of pure chitosan film and the CF-1 film. The results prove that iron ions can form metal coordination bonds with amino groups and hydroxyl groups on chitosan.

3.2 XPS analysis

To determine the surface composition of the CS, CHP-4 and CHPF-2 films, the X-ray photoelectron (XPS) spectra of the different films were obtained (Fig. 2). It can be seen from the full spectrum results in Fig. 2(a) that the energy peaks of N 1s of the CHP-4 film and CHPF-2 film were enhanced after the addition of HPEI. In the chitosan-based film spectra, the C 1s peak was divided into peaks at 284 eV, 286 eV, and 288 eV, corresponding to the C–C bond, C–N/C–O bond and C=O bond, respectively.[6] In the CS and CHP-4 spectra, the peak at 286 eV showed that CHP-4 was stronger than CS, which was caused by the addition of HPEI. Fig. 4(d) shows that the intensity of CHPF-2 was weaker than that of CHP-4 at the peak of 286 eV. It can be ascribed to the formation of the metal coordination bond between Fe^{3+} and the amino group in the internal network.

3.3 Morphology of the films

Fig. 3 and 4 exhibit the SEM images of the tensile fracture surfaces of the CS film, CHP films and CHPF films. The cross section of the CS film suggested that the internal structure of it was very compact. After HPEI was added, some pore structures began to appear in the cross section, which may be caused by the evaporation of water vapor during film formation. Moreover, HPEI is a hyperbranched molecule, and occupied a larger spatial conformation in the internal structure. Meanwhile, the cross-sectional structure was more regular under the condition of high proportion of HPEI. It can be illustrated that the strong connection between the chitosan matrix molecules was broken after the addition of HPEI. As shown in Fig. 4, after Fe^{3+} was

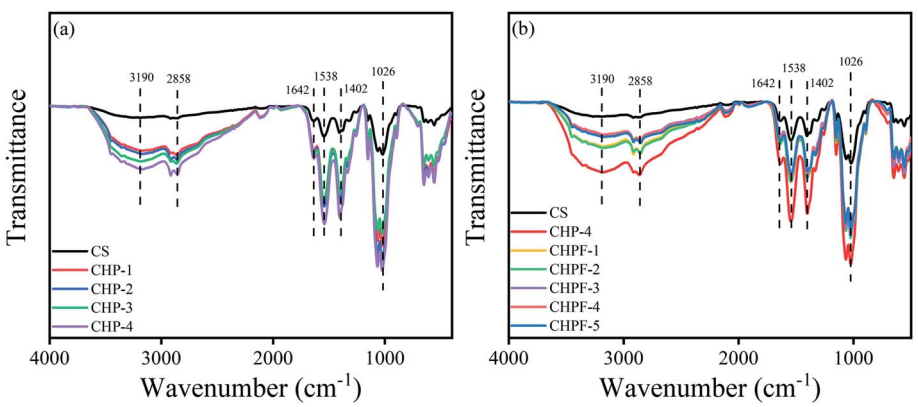

Fig. 1 (a) FT-IR spectra of the CS and CHP films. (b) FT-IR spectra of the CS, CHP-4 and CHPF films.

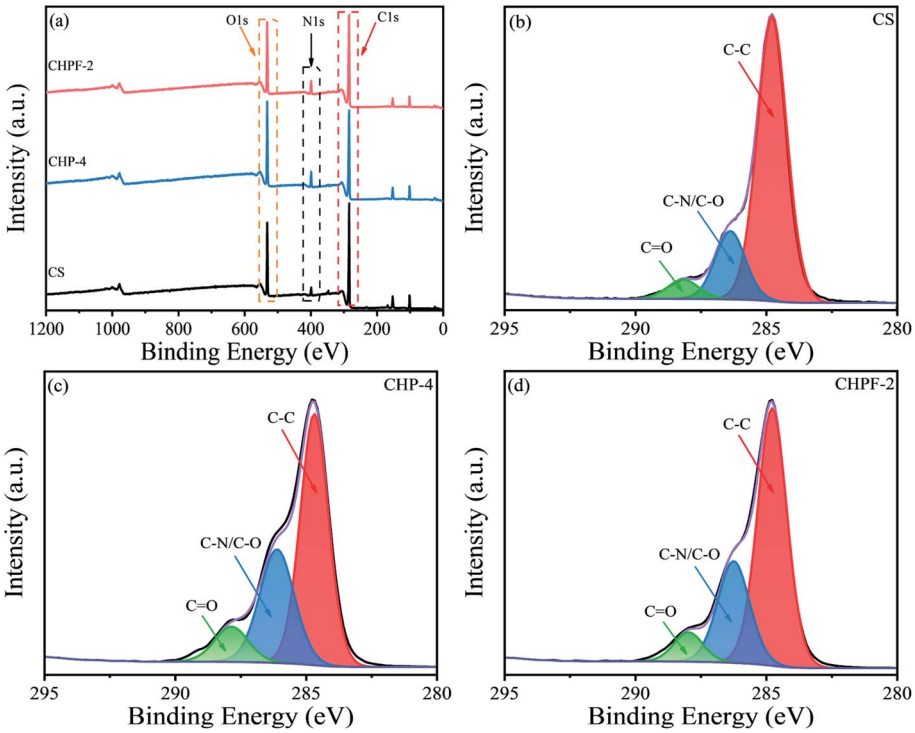

Fig. 2 XPS spectra of the CS, CHP-4 and CHPF-2 films: (a) the wide-range spectra, (b) C 1s region of the CS film, (c) C 1s region of the CHP-4 film, and (d) C 1s region of the CHPF-2 film.

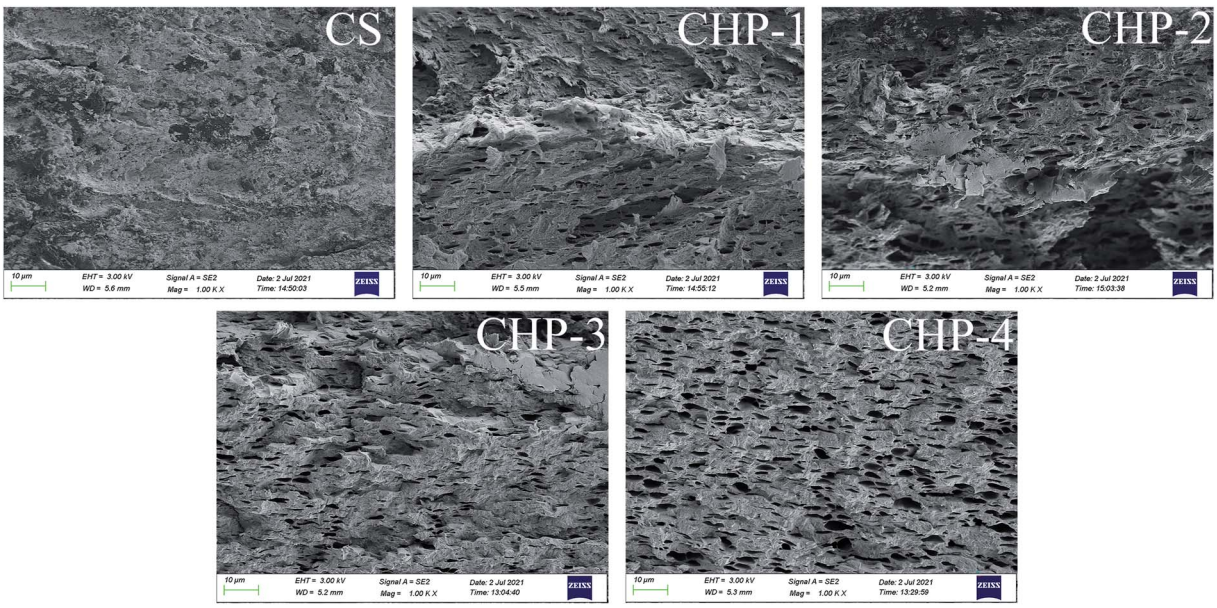

Fig. 3 SEM images (tensile fracture surface) of the CS and CHP films.

added, the pore structures of the CHPFs films decreased and became dense. This phenomenon can be demonstrated by the introduction of metal coordination; a metal coordination network was constructed between Fe^{3+}, chitosan, and the HPEI molecules. Compared with the other CHPF films, the CHPF-2 film exhibited a more uniform structure, which was attributed to the synergistic effect of the internal hydrogen bond network and the metal coordination network. However, the structure of the CHPF3, CHPF-4 and CHPF-5 films is relatively uneven compared to that of CHPF-2, which may be due to the formation of too many metal coordination bonds and the breaking of the internal hydrogen bond network. Combined with the SEM data and the mechanical stretching results (Fig. 6), it can be demonstrated that the addition of HPEI formed a dense

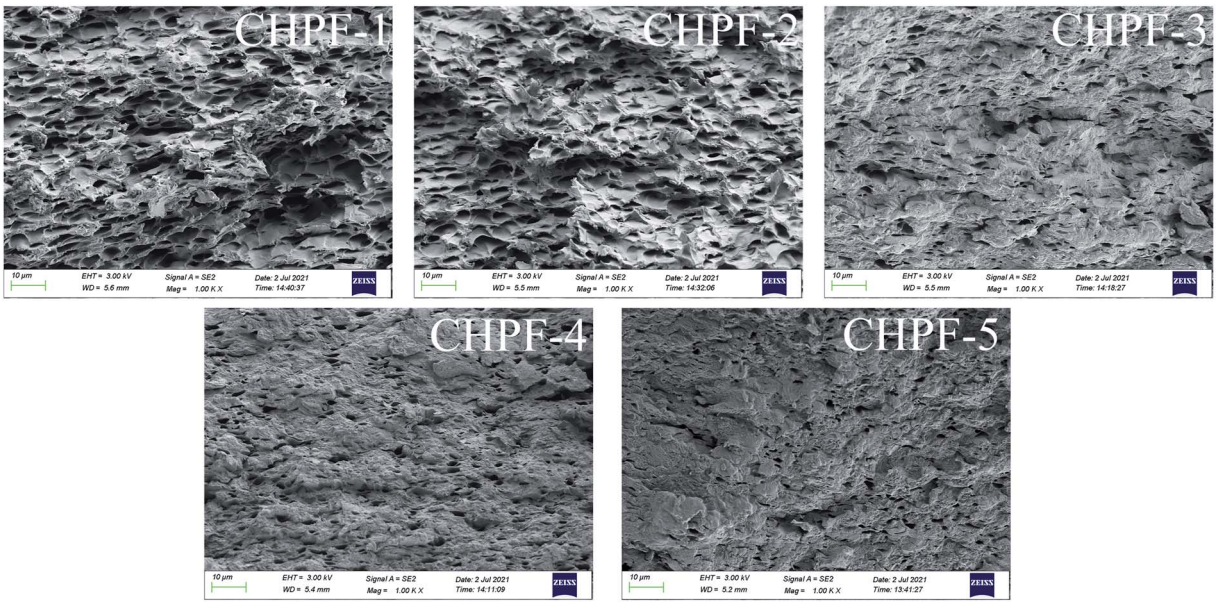

Fig. 4 SEM images (tensile fracture surface) of the CHPF films.

hydrogen bond interaction between HPEI and chitosan molecules, such that the internal structure of the film was uniform and the film exhibited good toughness. When metal coordination bonds were introduced into the network, a portion of the hydrogen bonds in the internal network acted as sacrificial bonds, resulting in an increase in the tensile strength of the film but a decrease in strain.

3.4 Thermal stability

The TGA and DTG results of CS, CHP-4 and CHPF-2 are presented in Fig. 5. For the CS film, the mass loss was between 250 and 400 °C, mainly because of the loss of the CS chain.[36] Meanwhile, the residual rate of the chitosan film remained above 39.4%. The thermal degradation temperature of the CHP-2 film after adding HPEI increased from 279.8 °C to 293.4 °C, but the residual rate decreased from 39.4% to 33.9%. The increase in thermal degradation temperature suggested that the addition of HPEI could change the internal network structure, form a large number of hydrogen bonds, and improve the thermal stability of the CHP-4 film. Compared with the CHP-4 film, the thermal degradation temperature of the CHPF-2 film increased a little. This can be explained by the very small amount of metal ions added, and the formation of metal coordination bonds destroys the hydrogen bonds between HPEI and chitosan molecules. The residual mass rate of the CHPF-2 film was slightly higher than that of the CHP-4 film. This may be due to the addition of iron ions, which react under high temperature conditions to generate a small amount of iron compounds.

3.5 Mechanical properties of the chitosan-based films

According to the stress–strain curves (Fig. 6), the tensile strength of the pure chitosan (CS) film was 54.1 MPa but the failure train was only 10.3 ± 0.2%, which would restrict its application. After adding different contents of HPEI, the results showed that the strain of the CHP films was tunable. The typical

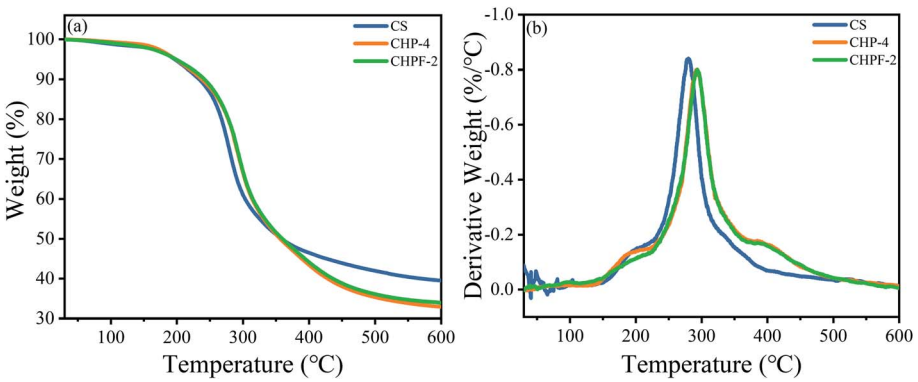

Fig. 5 (a) TGA curves and (b) DTG curves of the CS, CHP-4, and CHPF-2 films.

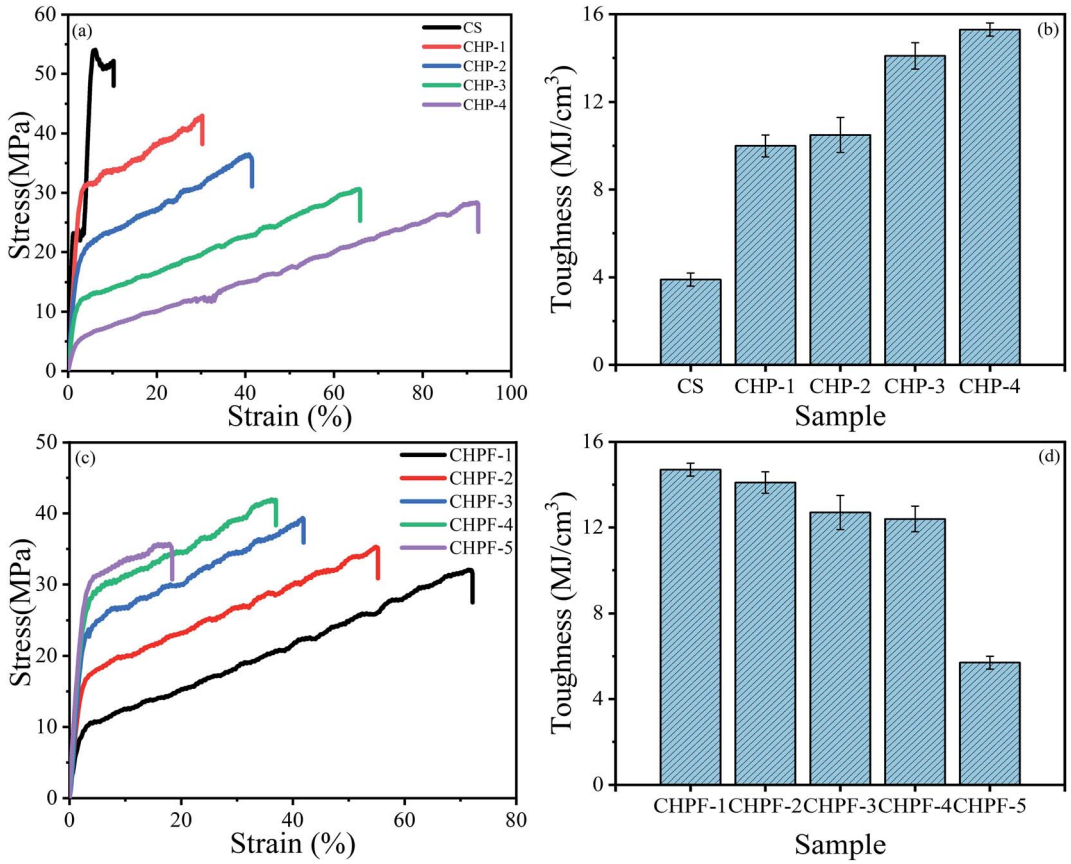

Fig. 6 (a) Stress–strain curves and (b) toughness of the CS and CHP films. (c) Stress–strain curves and (d) toughness of the CHPF films.

parameters are summarized in Table 1. The tensile strength of the CHP-1, CHP-2, CHP-3, and CHP-4 films decreased to 44.1 MPa, 36.4 MPa, 30.5 MPa, and 28.3 MPa, respectively, but the strain of the CHP films increased to 30.3%, 41.5%, 65.7%, and 92.5%, respectively. Compared with that of pure chitosan film, the strain of CHP-1, CHP-2, CHP-3, and CHP-4 increased by 194.2%, 302.9%, 537.9%, and 798.1%, respectively. This can be attributed to the construction of a hydrogen bond network in the internal network that was introduced by HPEI. Scheme 2 reveals that in the internal structure of the CHP films, a strong hydrogen bond network was formed between chitosan and HPEI. During stretching, the long-chain chitosan molecules and HPEI molecular chains were stretched first, followed by the hydrogen bond network. As presented in Fig. 6(b), the toughness of the CHP-4 film was about 3.9 times that of pure chitosan film (3.9 ± 0.3 MJ m^{-3}).

The introduction of Fe^{3+} into the CS/HPEI homogeneous solution promoted the formation of metal coordination bonds between iron ions, chitosan, and HPEI. The color of the evenly stirred solution changed to reddish brown, which indicated the formation of metal-amino coordination bonds. Table 2 summarizes the specific test results. It was observed from the results that the tensile strength of the film increased but the strain decreased after adding a small amount of iron ions. The reason for this phenomenon could be the formation of metal coordination bonds that sacrifice a part of the hydrogen bond network, which leads to strain reduction in the CHPF films. As shown in Scheme 2, the formation of metal coordination bonds sacrificed a part of the hydrogen bonds, and the presence of metal coordination bonds limits the extension of chitosan and HPEI molecular chains during the stretching process. The results in Fig. 6(c) reveal that after adding more Fe^{3+}, the tensile

Table 1 Mechanical properties of the CS and CHP films

Sample code	Ultimate stress (MPa)	Ultimate strain (%)	Toughness (MJ m^{-3})	Young's modulus (MPa)
CS	54.1 ± 0.5	10.3 ± 0.2	3.9 ± 0.3	1625.4 ± 65.8
CHP-1	44.1 ± 1.2	30.3 ± 0.8	10.0 ± 0.5	1364.1 ± 48.6
CHP-2	36.4 ± 0.5	41.5 ± 1.9	10.5 ± 0.8	721.9 ± 29.8
CHP-3	30.5 ± 0.6	65.7 ± 5.0	14.1 ± 0.6	107.7 ± 3.4
CHP-4	28.3 ± 0.8	92.5 ± 7.6	15.3 ± 0.3	43.7 ± 1.8

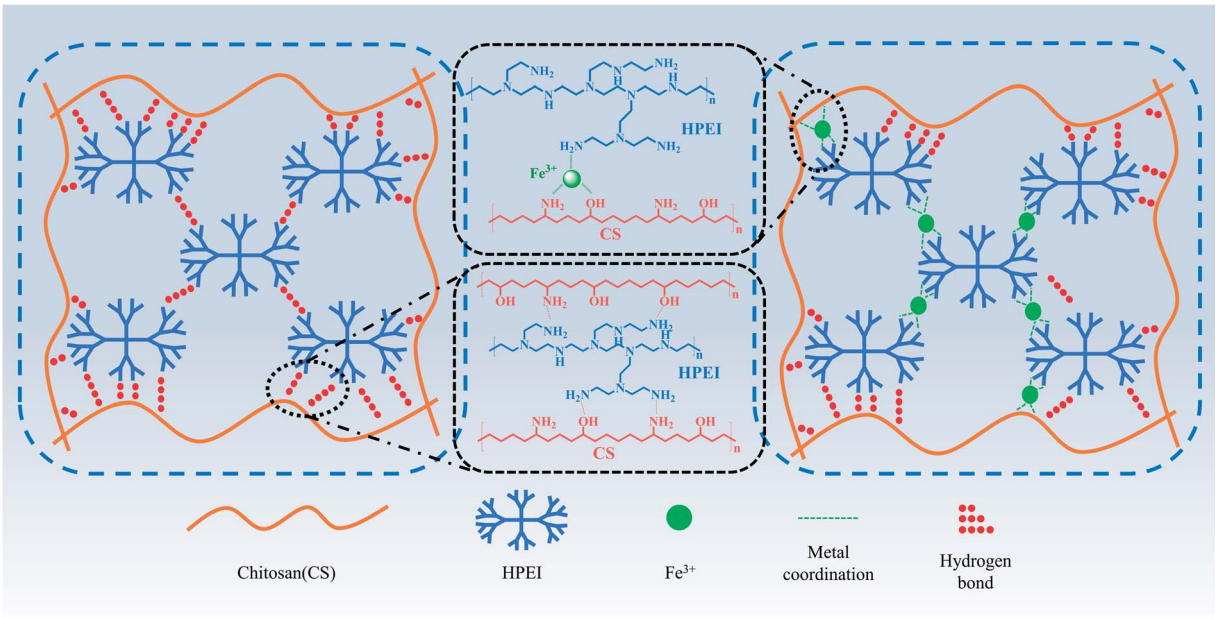

Scheme 2 Schematic diagram of the internal structure of the CHP and CHPF films.

Table 2 Mechanical properties of the CHPF films

Sample code	Ultimate stress (MPa)	Ultimate strain (%)	Toughness (MJ m^{-3})	Young's modulus (MPa)
CHPF-1	32.1 ± 0.5	72.2 ± 0.2	14.7 ± 0.3	95.2 ± 2.3
CHPF-2	35.3 ± 1.2	55.2 ± 0.8	14.1 ± 0.5	436.2 ± 18.7
CHPF-3	39.3 ± 0.5	41.9 ± 1.9	12.7 ± 0.8	758.8 ± 35.2
CHPF-4	42.0 ± 0.6	37.0 ± 5.0	12.4 ± 0.6	1040.5 ± 42.8
CHPF-5	35.7 ± 0.8	18.4 ± 7.6	5.7 ± 0.3	1107.3 ± 55.1

strength of the CHPF-5 film decreased and the strain was reduced. The existence of more metal coordination bonds, which lead to the destruction of the double network (metal coordination and hydrogen bond) structure, can be illustrated.

3.6 UV measurement

Fig. 7 exhibits the UV-visible measurement results of the HPEI, CS, CHP, and CHPF solutions. As shown in Fig. 7(a), the HPEI solution exhibits no absorption peak at 300 nm, while the CS solution exhibits a peak at 300 nm. After HPEI was added to the chitosan solution, the absorption peak of the CHP solution at 300 nm was enhanced. The results in Fig. 7(b) exhibit that the intensity of the absorption peak at 365 nm improved with the increase of iron ion content. Fig. 7(d) shows that the transmittance of the CHP-4 solution at 365 nm was 67.8%, and the transmittance of the CHPF-2 solution at 365 nm was 33.4%. The light transmittance values of the CHPF-3, CHPF-4, and CHPF-5 solutions at 365 nm were 17.6%, 7.6%, and 1.7%, respectively. This result showed that the CHPF solutions have good UV resistance after adding iron ions. It can be seen from Scheme 1 that the color of the CS film was light yellow, the color of the CHP-4 film was light brown, and the color of the CHPF-2 film was dark brown. With the addition of HPEI and iron ions, the colors of the films became darker, from light yellow to dark brown (Scheme 1).

3.7 Fluorescence property

From the result of the fluorescence spectra of the CS and CHP solutions, the pure chitosan solution exhibited a very strong fluorescence emission, and the emission peak appeared at around 465 nm (Fig. 8). In addition, compared with the pure chitosan solution, the fluorescence intensities of the CHP-1, CHP-2, CHP-3, and CHP-4 solutions were stronger. Chitosan, with hydroxyl, amino and acetylamino groups, can provide useful through-space intermolecular and intramolecular interactions among the groups and provide a rigid conformation simultaneously.[2] On the other hand, with the addition of HPEI, there were a large number of hydrogen bonds in the CHP structure, which not only rigidify the molecular conformation but also promote the through-space conjugation among adjacent n and π electrons, further improving the fluorescence intensity.[2] The fluorescence emission intensities of the CHP-3 and CHP-4 solutions were similar, revealing that the addition of more HPEI can slightly enhance the fluorescence intensity.

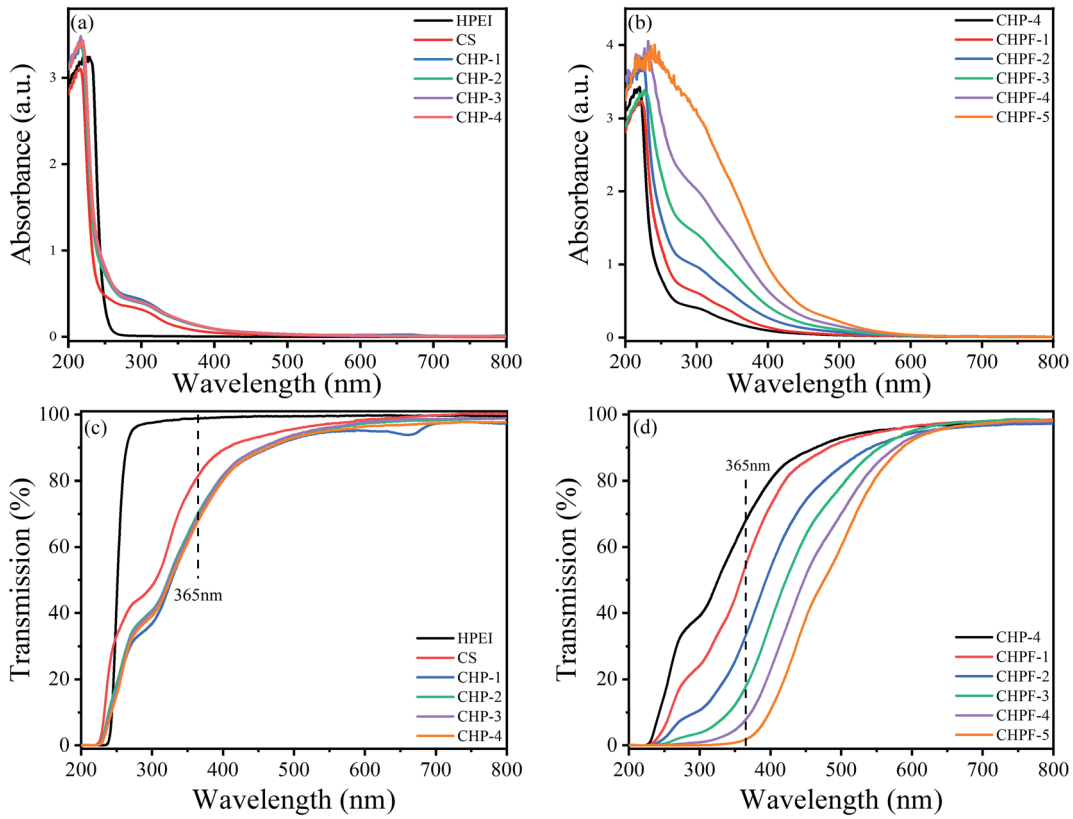

Fig. 7 (a) UV-vis absorption spectra of the HPEI, CS and CHP solutions. (b) UV-vis absorption spectra of the CHP-4 and CHPF solutions. (c) UV-vis transmission spectra of the HPEI, CS and CHP solutions. (d) UV-vis transmission spectra of the CHP-4 and CHPF solutions.

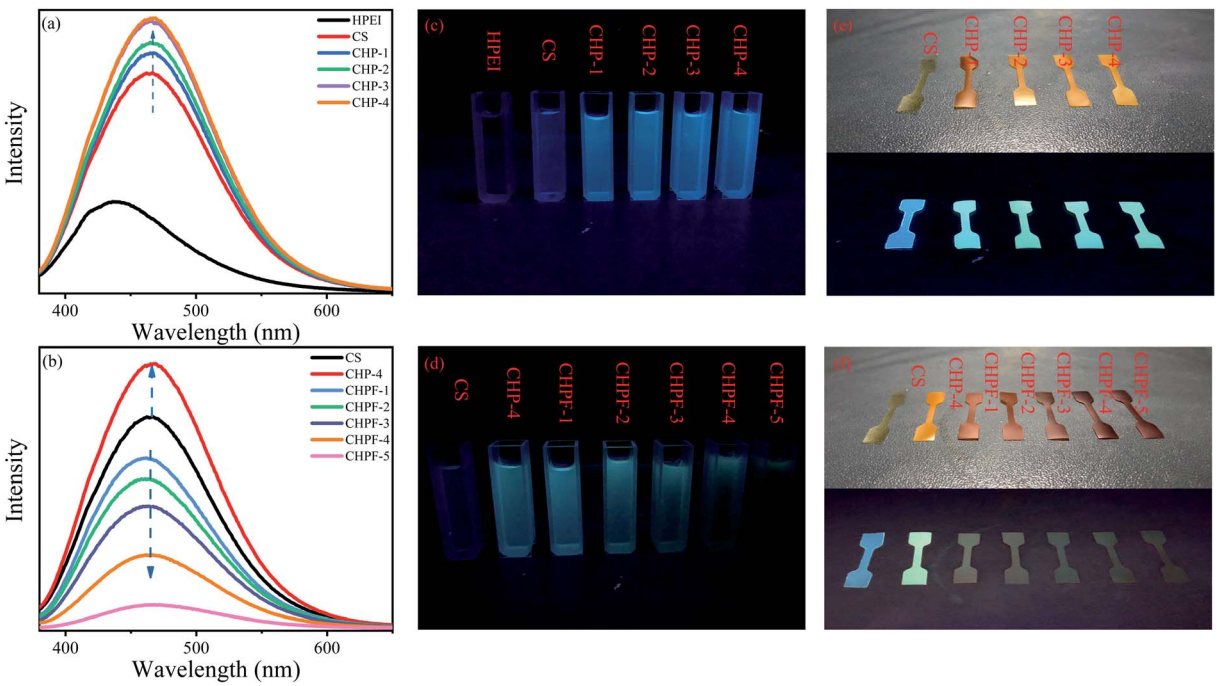

Fig. 8 (a) and (b) Fluorescence spectra of the HPEI, CS, CHP1-4 and CHPF1-5 solutions (10 mg mL^{-1}) under a 365 nm excitation wavelength. (c) and (d) Fluorescence photographs of the HPEI, CS, CHP1-4 and CHPF1-5 solutions (10 mg mL^{-1}) under 365 nm ultraviolet light. (e) and (f) Fluorescence photographs of the CS, CHP1-4 films and CHPF1-5 films under 365 nm ultraviolet light.

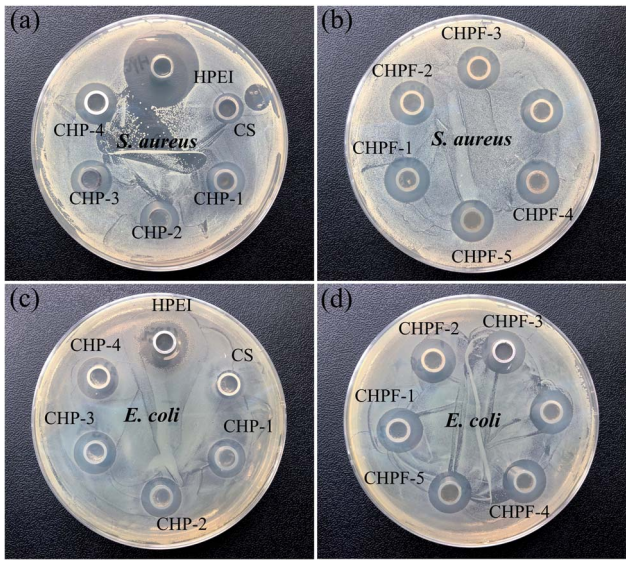

Fig. 9 (a–d) Zone of inhibition (ZOI) of CS, CHP, and CHPF against *S. aureus* and *E. coli*.

Fe^{3+} is paramagnetic and has a strong quenching effect on fluorescence.[40,41] From the results of the fluorescence spectra (Fig. 8), the fluorescence intensity gradually decreased with continuous addition of Fe^{3+} in the CHP-4 solution. Due to the addition of Fe^{3+}, a metal coordination bond was formed between Fe^{3+} and the negatively charged groups, which destroy the hydrogen bond network in CHP-4, resulting in a decrease of fluorescence intensity. It can be seen from the figure that when the amount of iron ions reaches 6 mg, the solution of CHPF-5 has almost no fluorescence intensity. Therefore, CHP-4 can be used as a biosensor for detecting Fe^{3+}. Conversely, the decrease of fluorescence intensity also demonstrated the formation of metal coordination bonds.

3.8 Antibacterial property

Oxford cup tests were employed to investigate the antibacterial activity of the CS film, CHP films and the CHPF films against *S. aureus* and *E. coli*.[42] With the introduction of HPEI, the diameter of the inhibition zone of the CHP films for *S. aureus* and *E. coli* increases and the inhibition zone diameter remains basically the same (Fig. 9). The diameter of the inhibition zone of CS against *S. aureus* was 9.58 mm, and the diameter of the inhibition zone of the CHP films was 12.38 mm, 12.55 mm, 12.67 mm and 12.69 mm, respectively. After adding iron ions, the diameters of the inhibition zones of the CHPF films were 13.08 mm, 13.03 mm, 13.04 mm, 13.02 mm, and 12.98 mm, respectively. The diameter of the inhibition zone of CS to *E. coli* was 9.36 mm, and the diameters of the inhibition zones of the CHP films were 12.31 mm, 12.45 mm, 12.56 mm and 12.61 mm, respectively. After adding iron ions, the diameters of the inhibition zones of the CHPF films were 13.07 mm, 13.05 mm, 13.04 mm, 13.02 mm, and 12.99 mm, respectively. It has been determined that there are different compounds in the arrangement of Gram-positive and Gram-negative cell walls.[43] After HPEI was added, the antibacterial activity against *S. aureus* was improved because the peptidoglycan layer was thicker than that of Gram-negative bacteria, which will eventually reduce the penetration of the film solution to the cell wall of Gram-positive bacteria. The increased antibacterial activity against *E. coli* may be due to the interaction between the positive charge of the amine group in HPEI and the mainly anionic lipopolysaccharides on the cell surface.[43] After that, the addition of iron ions did not significantly enhance the antibacterial performance. This might be illustrated by the fact that the added amount of iron ions was very small, and the antibacterial properties of the films were almost unimproved.

4 Conclusion

In summary, chitosan-based films with high mechanical performances were prepared by a facile design strategy. Characterization of films was carried out using different analytical techniques to evaluate the effect of HPEI and Fe^{3+} on CS films. Introducing HPEI can significantly enhance the toughness and strain of CS films by forming a single hydrogen bond network. The toughness and strain of CHP films increased from 3.9 MJ m^{-3}, 10.3% to 15.3 MJ m^{-3}, 92.5% after the addition of 20% HPEI. After adding iron ions, the tensile strength of the chitosan-based films would further be improved due to the synergistic effect of hydrogen bonds and metal coordination bonds—a double noncovalent network. Meanwhile, with the addition of HPEI and Fe^{3+}, the chitosan-based films exhibited distinct antibacterial activity against *S. aureus* and *E. coli.* Fluorescence spectroscopy further verified the fluorescent properties of the chitosan-based films. After the addition of iron ions, the fluorescence intensity decreases, and the CHP films can be used as biosensors to detect the concentration of Fe^{3+} in the environment. Therefore, we believe that chitosan-based materials with multifunctions will provide a new platform for a variety of applications.

Conflicts of interest

The authors declare that they have no known competing financial interests or personal relationships that could have appeared to influence the work reported in this paper.

Acknowledgements

This research was supported by the Fundamental Research Funds for the National Natural Science Foundation of China (Project 31760188).

References

1 S. Takeshita, S. Zhao, W. J. Malfait and M. M. Koebel, *Angew. Chem., Int. Ed.*, 2021, **60**, 9828–9851.
2 Z. Dong, H. Cui, Y. Wang, C. Wang, Y. Li and C. Wang, *Carbohydr. Polym.*, 2020, **227**, 115338.
3 Z. Chang, S. Zhang, F. Li, Z. Wang, J. Li, C. Xia, Y. Yu, L. Cai and Z. Huang, *Chem. Eng. J.*, 2021, **404**, 126505.

4 H. Wang, J. Qian and F. Ding, *J. Agric. Food Chem.*, 2018, **66**, 395–413.
5 W. Cao, J. Yan, C. Liu, J. Zhang, H. Wang, X. Gao, H. Yan, B. Niu and W. Li, *Carbohydr. Polym.*, 2020, **247**, 116643.
6 P. K. Panda, J.-M. Yang and Y.-H. Chang, *Carbohydr. Polym.*, 2021, **257**, 117633.
7 F. Gabriele, A. Donnadio, M. Casciola, R. Germani and N. Spreti, *Carbohydr. Polym.*, 2021, **251**, 117106.
8 Q. Yu, Y. Song, X. Shi, C. Xu and Y. Bin, *Carbohydr. Polym.*, 2011, **84**, 465–470.
9 M. Shojaee Kang Sofla, S. Mortazavi and J. Seyfi, *Carbohydr. Polym.*, 2020, **232**, 115784.
10 A. S. Soubhagya, A. Moorthi and M. Prabaharan, *Int. J. Biol. Macromol.*, 2020, **157**, 135–145.
11 S. Yadav, G. K. Mehrotra and P. K. Dutta, *Food Chem.*, 2021, **334**, 127605.
12 D. Kadam, B. Momin, S. Palamthodi and S. S. Lele, *Carbohydr. Polym.*, 2019, **211**, 124–132.
13 X. Zhang, Y. Liu, H. Yong, Y. Qin, J. Liu and J. Liu, *Food Hydrocolloids*, 2019, **94**, 80–92.
14 J. Liu, J. Huang, Z. Hu, G. Li, L. Hu, X. Chen and Y. Hu, *Int. J. Biol. Macromol.*, 2021, **189**, 363–369.
15 Y. Qin, Y. Liu, L. Yuan, H. Yong and J. Liu, *Food Hydrocolloids*, 2019, **96**, 102–111.
16 M. M. Rahman, M. S. Islam and G. S. Li, *Polym. Test.*, 2018, **68**, 302–308.
17 S. Mallakpour and S. Rashidimoghadam, *Int. J. Biol. Macromol.*, 2020, **144**, 389–402.
18 E. Kolanthai, P. A. Sindu, D. K. Khajuria, S. C. Veerla, D. Kuppuswamy, L. H. Catalani and D. R. Mahapatra, *ACS Appl. Mater. Interfaces*, 2018, **10**, 12441–12452.
19 Y. Yang, H. Zhu, J. Wang, Q. Fang and Z. Peng, *ACS Appl. Mater. Interfaces*, 2018, **10**, 33493–33506.
20 Y. Liu, Z. Cai, L. Sheng, M. Ma, Q. Xu and Y. Jin, *Carbohydr. Polym.*, 2019, **215**, 348–357.
21 S. Bratskaya, Y. Privar, D. Nesterov, E. Modin, M. Kodess, A. Slobodyuk, D. Marinin and A. Pestov, *Biomacromolecules*, 2019, **20**, 1635–1643.
22 N. A. Negm, H. H. H. Hefni, A. A. A. Abd-Elaal, E. A. Badr and M. T. H. Abou Kana, *Int. J. Biol. Macromol.*, 2020, **152**, 681–702.
23 M. Bhattacharjee, N. B. Pramanik, N. K. Singha and D. J. Haloi, *Polym. Chem.*, 2020, **11**, 6718–6738.
24 W. Huang, Y. Wang, S. Zhang, L. Huang, D. Hua and X. Zhu, *Macromolecules*, 2013, **46**, 814–818.
25 C. Chen, M. Liu, C. Gao, S. Lü, J. Chen, X. Yu, E. Ding, C. Yu, J. Guo and G. Cui, *Carbohydr. Polym.*, 2013, **92**, 621–628.
26 S. Bi, P. Wang, S. Hu, S. Li, J. Pang, Z. Zhou, G. Sun, L. Huang, X. Cheng, S. Xing and X. Chen, *Carbohydr. Polym.*, 2019, **224**, 115176.
27 Monika, A. K. Pal, S. M. Bhasney, P. Bhagabati and V. Katiyar, *ACS Omega*, 2018, **3**, 13298–13312.
28 C. E. Tanase and I. Spiridon, *Mater. Sci. Eng. C*, 2014, **40**, 242–247.
29 F. Li, Q. Ye, Q. Gao, H. Chen, S. Q. Shi, W. Zhou, X. Li, C. Xia and J. Li, *ACS Appl. Mater. Interfaces*, 2019, **11**, 16107–16116.
30 J. Yang, M. Li, Y. Wang, H. Wu, T. Zhen, L. Xiong and Q. Sun, *Biomacromolecules*, 2019, **20**, 801–812.
31 C. Liu, D. J. McClements, M. Li, L. Xiong and Q. Sun, *J. Agric. Food Chem.*, 2019, **67**, 6508–6516.
32 K. Fukao, T. Nonoyama, R. Kiyama, K. Furusawa, T. Kurokawa, T. Nakajima and J. P. Gong, *ACS Nano*, 2017, **11**, 12103–12110.
33 J. Ren, H. Xuan and L. Ge, *Appl. Surf. Sci.*, 2019, **469**, 213–219.
34 N. Holten-Andersen, M. J. Harrington, H. Birkedal, B. P. Lee, P. B. Messersmith, K. Y. C. Lee and J. H. Waite, *Proc. Natl. Acad. Sci.*, 2011, **108**, 2651.
35 D. Zhang, F. Yang, J. He, L. Xu, T. Wang, Z.-Q. Feng, Y. Chang, X. Gong, G. Zhang and J. Zheng, *ACS Appl. Polym. Mater.*, 2020, **2**, 1031–1042.
36 S. Roy and J.-W. Rhim, *Food Hydrocolloids*, 2020, **98**, 105302.
37 S. Shankar and J.-W. Rhim, *Food Hydrocolloids*, 2018, **82**, 116–123.
38 Q. Li, J. Zhou and L. Zhang, *J. Polym. Sci., Part B: Polym. Phys.*, 2009, **47**, 1069–1077.
39 P. Mujeeb Rahman, K. Muraleedaran and V. M. A. Mujeeb, *Int. J. Biol. Macromol.*, 2015, **77**, 266–272.
40 A. Barba-Bon, A. M. Costero, S. Gil, M. Parra, J. Soto, R. Martínez-Máñez and F. Sancenón, *Chem. Commun.*, 2012, **48**, 3000–3002.
41 L. Qiu, C. Zhu, H. Chen, M. Hu, W. He and Z. Guo, *Chem. Commun.*, 2014, **50**, 4631–4634.
42 M. Moghadam, M. Salami, M. Mohammadian, M. Khodadadi and Z. Emam-Djomeh, *Food Hydrocolloids*, 2020, **104**, 105735.
43 A. L. Mohamed and A. G. Hassabo, *Int. J. Biol. Macromol.*, 2021, **170**, 479–489.